Journal of Materials Chemistry A

Accepted Manuscript

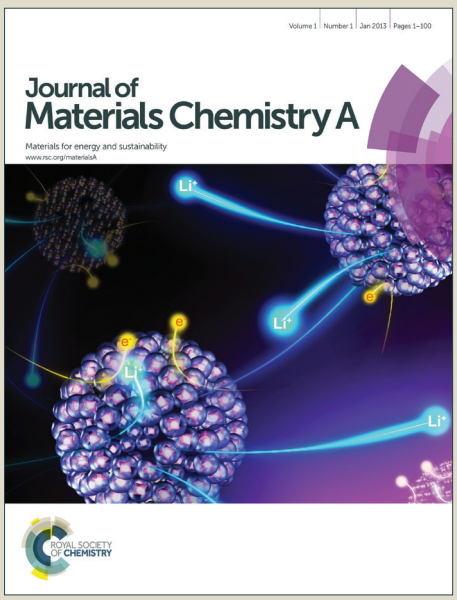

ROYAL SOCIETY OF CHEMISTRY

www.rsc.org/materialsA

Journal of Materials Chemistry A RSCPublishing

ARTICLE

Fabrication of Hybrid Polymer/Metal Organic Framework Membranes: Mixed Matrix Membranes versus In-Situ Growth

Cite this: DOI: 10.1039/x0xx00000x

Received 00th January 2012,
Accepted 00th January 2012

DOI: 10.1039/x0xx00000x

www.rsc.org/

James Campbell[a,b], György Székely[a], R.P. Davies[b], D. Christopher Braddock[b], Andrew G. Livingston[a]*

Hybrid polymer/metal organic framework (MOF) membranes have been prepared using either a mixed matrix membrane (MMM) or in-situ growth (ISG) approach and were evaluated for application in organic solvent nanofiltration (OSN). MMMs were produced by dispersing pre-formed particles of the MOF HKUST-1 in polyimide P84 dope solutions. MMMs demonstrated both (i) higher rejections of styrene oligomers and (ii) lower flux decline than the polymeric control membranes. Furthermore, an alternative hybrid membrane fabrication methodology – in-situ growth (ISG) of HKUST-1 in integrally skinned asymmetric polymer membrane supports – has been successfully demonstrated. Ultrafiltration support membranes were submerged in HKUST-1 precursor solutions in order to promote the growth of MOF within the porous structure of the polymer membranes. The presence of HKUST-1 in the membranes was proven with X-ray powder diffraction (XRPD). Energy-dispersive X-ray spectroscopy (EDX) was used to reveal the distribution of HKUST-1 throughout the ISG membranes, and was found to be even across the surface and throughout the cross-section. The ISG membranes also had higher solute rejections and lower flux decline than the MMMs.

1. Introduction

Organic solvent nanofiltration (OSN) is a pressure driven filtration technology that can separate on a molecular level, based on size, shape and/or chemical potential. The most common membranes used for OSN applications are integrally skinned asymmetric polymer membranes. These membranes consist of a thin, dense, selective separation layer on top of a porous support layer of the same material. The advantages of integrally skinned asymmetric polymer membranes include their flexibility, durability and ease of production. Integrally skinned asymmetric polymer membranes are designed to be flexible so they can be used within membrane modules e.g. spiral wound membrane modules[1]. The most common preparation methodology for producing integrally skinned asymmetric polymer membranes is phase inversion via immersion precipitation[1] (see **Figure 1**). Polyimide membranes resistant to aprotic solvents such as DMF have been fabricated via the process of cross-linking[2, 3]. The properties of polyimide membranes have been controlled by altering parameters such as membrane casting thickness, annealing time and solvent/co-solvent ratio[4, 5]. Unfortunately control of the phase inversion process is imprecise, and membranes with predictable, regular porous structures cannot be obtained. Another negative aspect of polymer membranes is flux decline, caused by pressure induced compaction and rearrangement of the polymer chains[6, 7]. Both flux decline and irregular porous structures have been obstacles to producing polymer OSN membranes with precise and predicable separation performances.

One approach to reduce flux decline has been to produce hybrid organic/inorganic membranes using a mixed matrix membrane (MMM) approach. Titanium dioxide has been added to integrally skinned asymmetric polymer membranes to produce MMMs used to combat flux decline in OSN[8]. Another inorganic material organosiloxane has also been used to reduce the effect of flux decline in OSN membranes[7].

MMMs were originally developed for gas separation processes[9-16]. MMMs are made by dispersing particles of inorganic material in polymer membrane dope solutions[17] (see **Figure 1**). This membrane fabrication methodology leads to the formation of hybrid membranes with discrete inorganic particles distributed in a continuous polymer phase[17]. Metal organic frameworks (MOFs) could be used in MMMs to enhance the performance of OSN membranes.

MOFs are crystalline materials consisting of metal ions or metal ion clusters, connected by organic ligands to form a continuous regular network[18, 19]. Many MOFs have been found to have highly porous structures [19-22] and therefore could be suitable for OSN separations. However due to their crystalline nature, pure MOF membranes are inflexible and brittle, and thus unsuitable for use in membrane modules. Hybrid polymer/MOF membranes (e.g. MMMs) could be produced utilising the flexibility and mechanical strength of polymer membranes while incorporating the separation potential of MOFs.

MMMs containing MOFs have been produced for application in OSN; their porous nature utilised to improve the performance of thin film composite membranes[23, 24]. In this work MMMs containing the metal organic framework (MOF) HKUST-1, also known as Cu_3BTC_2 (BTC = benzene tricarboxylate), in an integrally skinned asymmetric polyimide membrane are fabricated with a view to testing the effect of the

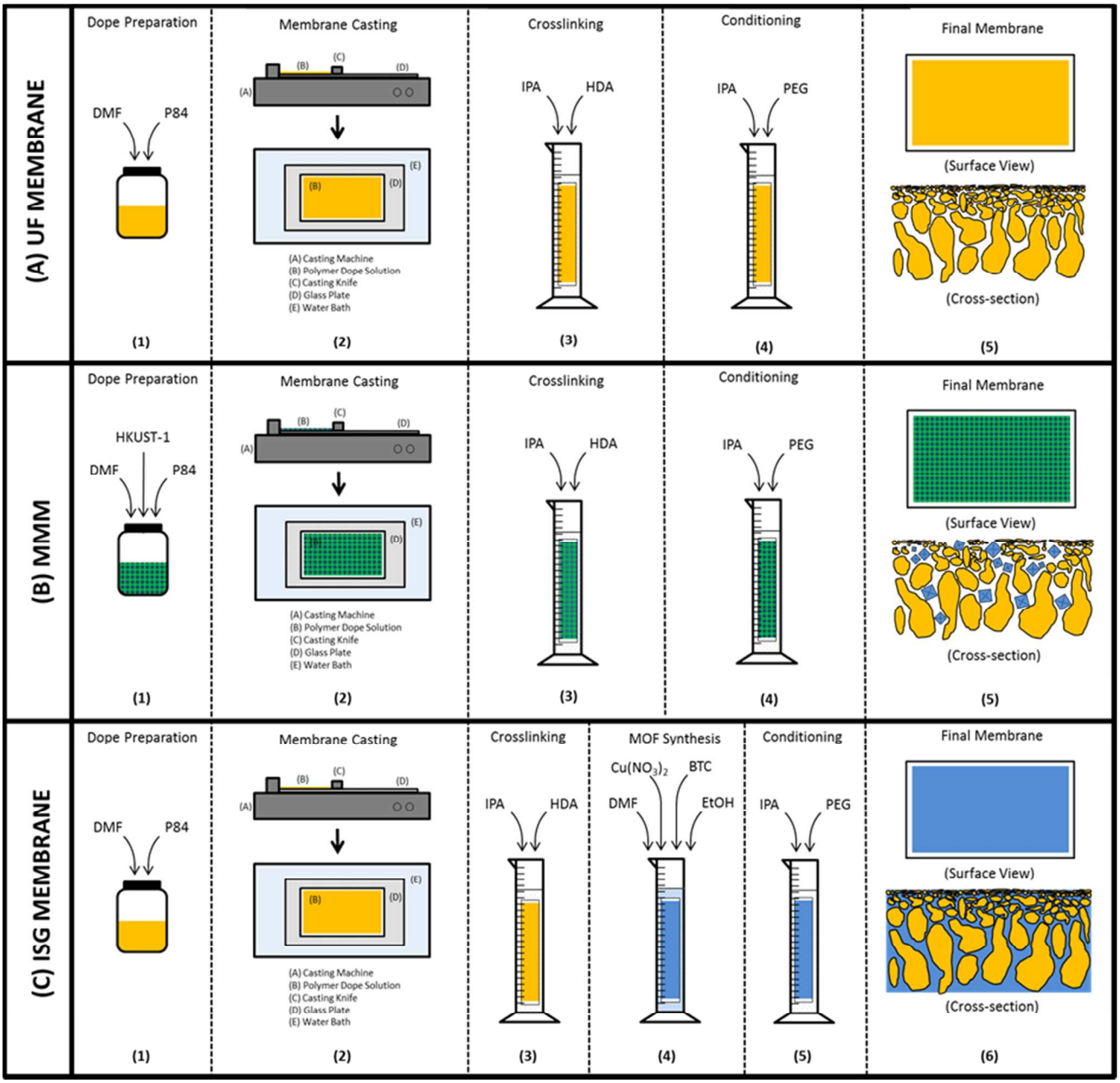

Figure 1: Schematic of membrane fabrication processes (A) UF membrane, (B) MMM and (C) ISG membrane; (A) shows the fabrication of a integrally skinned asymmetric polymer membrane formed via phase inversion, the final membrane is purely polymeric with an irregular porous structure, (B) shows the fabrication of a MMM, pre-formed HKUST-1 crystals are added to the dope solution, producing a hybrid membrane with discrete particles of MOF in an irregular porous network, (C) shows the fabrication of the novel ISG membrane, where HKUST-1 is grown in-situ in the pores of integrally skinned asymmetric polymer membranes

MOFs on the performance of the membrane and flux decline in OSN applications.

HKUST-1 has been used to produce MMMs for gas separations and OSN[9-11, 23]. Transport through MMMs can be modelled using the Maxwell model[25-30] or other models such as the Bruggeman model[28, 29]. As MMMs contain discrete particles of MOF in a continuous polymer network, the permeation flow path through these membranes is modelled as a composite of the permeability characteristics of the MOF and the polymer. This means that there is a limit to the influence the MOF can have on the permeation properties of MMMs. The interaction between the polymer and the MOF is very important to the transport properties of MMMs[17]. The Maxwell model assumes perfect interaction between the MOF and the polymer, however the formation of non-selective voids, rigid polymer layers and polymer incursion into the MOF can reduce the effectiveness of MMMs[23, 26, 31, 32].

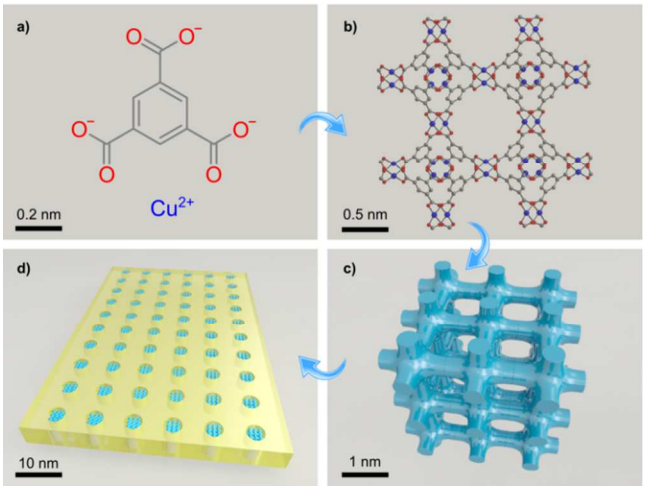

Figure 2: Schematic representation of ISG membrane showing (a) the building block molecules used to create HKUST-1, Cu^{2+} ions and benzene tricarboxylate, (b) a bird's eye view of the HKUST-1 molecular structure showing the window into the MOF cage, (c) a 3D rendering of a HKUST-1 crystal, showing the network of cages and (d) HKUST-1 crystals (blue) grown within the porous top layer of a polymer membrane (yellow)

To improve upon the performance of hybrid polymer/MOF membranes this work suggests a novel membrane fabrication method utilising *in-situ* growth (ISG) of MOF crystals in pre-formed polymer membranes. Using ISG to produce hybrid polymer/MOF membranes should minimise the issues of polymer/MOF interface interaction associated with MMMs. By growing MOF crystals in the pre-existing pores of the polymer membrane it is possible to grow a more continuous MOF phase. **Figure 2** shows MOF crystals grown in the top layer of a polymer membrane, transforming the membrane pores. The characteristics of these novel ISG membranes are tested with a number of analytical techniques (SEM, EDX, BET, AFM, XPRD, ATR-FTIR and water contact angle) to determine their structural properties. The novel ISG membranes are compared with MMMs and parallels are drawn between the membrane morphologies, permeance and rejection performance of the membranes.

HKUST-1 was selected in this work as it is one of the most widely studied and understood MOFs [18, 33] and can be fabricated at room temperature[34] from copper nitrate and 1,3,5-benzene tricarboxylic acid, or purchased from Sigma Aldrich as Basolite C300. In addition, the pore size of HKUST-1 (cage windows of 0.9 nm[35, 36]) is suitable for the OSN range.

2. Experimental

2.1. Materials

Polypropylene non-woven backing was supplied by Viledon, Germany. Polyimide polymer (Polyimide P84) powder was purchased from HP Polymer GmbH, Austria. Solvents used for membrane preparation and membrane testing isopropyl alcohol (IPA), acetone, dimethylformamide (DMF), ethanol (99.7%) and polyethylene glycol (MW 400) (PEG-400) were obtained from VWR international. Hexane-1,6-diamine for crosslinking was purchased from Sigma Aldrich. Copper nitrate trihydrate and 1,3,5-benzenetricarboxylic acid used for fabrication of HKUST-1 were purchased from VWR international. HKUST-1 powder was supplied by Sigma Aldrich under its commercial name Basolite C300. Polystyrene markers for solute rejection evaluation were purchased from Agilent Technologies, UK. All the chemicals were used as received without any further purification.

2.2. Membrane Preparation

2.2.1 Preparation of polymer ultrafiltration membranes
Polymer ultrafiltration membranes were produced via phase inversion. Dope solutions were formed by dissolving 24 wt% of polyimide P84, herein referred to as P84, in DMF (see step (A)1 in **Figure 1**). The P84 and the DMF were mixed in a sealed container, while the polymer dissolved, to ensure no moisture was absorbed into the dope solution. The dope solutions were cast on to polypropylene non-woven sheets using a casting knife set to a thickness of 250 µm, in a controlled environment with a temperature of 20 °C and a humidity of 30–40%. The polymer membranes were then precipitated from solution via immersion in water (see step (A)2 in **Figure 1**). The membranes were then placed in IPA to remove water from the polymer matrix. For crosslinking, the membranes were submerged in 30 $g.L^{-1}$ solutions of hexane-1,6-diamine (HDA) in IPA for 20 hours (see step (A)3 in **Figure 1**). After crosslinking the membranes were washed with IPA to remove excess crosslinking agent. Before testing, the membranes were conditioned with a PEG400:IPA (60:40 v/v) solution for 12 hours (see step (A)4 in **Figure 1**). Dense polymer ultrafiltration membranes were fabricated using the same methodology in an environment with a temperature of 15 °C and a humidity of 50-60%.

2.2.2. Preparation of hybrid polymer/MOF membranes MMM via dispersion of HKUST-1 particles in polymer dope solutions MMMs were prepared by dispersing HKUST-1 particles (average size 16 µm) in P84 dope solutions with 24 wt% of polymer in DMF (see step (B)1 in **Figure 1**). The ratio of polymer to MOF by weight in the dope solutions was 5:1. The HKUST-1 particles were mixed into the dope solution as the P84 dissolved. Mixing was undertaken in a sealed container to ensure no moisture was absorbed into the dope solution. The dope solutions were cast on to polypropylene non-woven sheets using a casting knife set to a thickness of 250 µm (see step (B)2 in **Figure 1**). The MMMs were then precipitated from solution via immersion in water. The membranes were then placed in IPA to remove water from the polymer matrix. For crosslinking, the membranes were submerged in 30 $g.L^{-1}$ solutions of HDA in IPA for 20 hours (see step (B)3 in **Figure 1**). After crosslinking the membranes were washed with IPA to remove excess crosslinking agent. Before testing the membranes were conditioned with a PEG400:IPA (60:40 v/v) solution for 12 hours (see step(B)4 in **Figure 1**). Dense MMMs was fabricated using the same methodology in an environment with a temperature of 15 °C and a humidity of 50-60%.

2.2.3. Preparation of hybrid polymer/MOF membranes via In-situ growth (ISG) of HKUST-1 Hybrid polymer/MOF *in-situ* growth (ISG) membranes were fabricated using polymer UF membranes as structural scaffolds (see section 2.2.1 and steps (C)1-3 in **Figure 1**). ISG membranes were prepared by immersing the polymer UF membranes into a fresh mixture of copper nitrate (0.86 M in Ethanol solution) and 1,3,5-benzenetricarboxylic acid (0.40 M in DMF solution) (see step (C)4 in **Figure 1**). The membranes were left stirring in solution for 24 hours, and then were extensively washed with DMF to remove any unreacted reagents. Before testing the membranes were conditioned with a PEG400:IPA (60:40 v/v) solution for 12 hours (see step (C)5 in **Figure 1**). To fabricate dense ISG membranes the same methodology was carried out using the dense polymer ultrafiltration membranes.

2.3. Membrane characterization

2.3.1. Membrane mass, density and thickness measurements Samples were taken from each membrane (area: 3 x 3 cm) and their thicknesses measured using a Mitutoyo electronic thickness gauge. The samples were then washed with acetone to remove PEG conditioning agent. The removal of PEG conditioning agent was confirmed using ATR-FTIR. The acetone was then dried from the membrane at room temperature. The mass of each sample was then measured using an electronic scale. The thickness and mass of the polypropylene non-woven backing was measured and subtracted from the thicknesses and masses of the membrane samples in order to find the dimensional parameters of the membrane alone.

2.3.2. ATR-FTIR Fourier Transform-Infrared (FT-IR) spectra were recorded on a Perkin-Elmer Spectrometer 100, with samples mounted on a zinc-selenium/diamond plate. The spectra were collected in the attenuated total reflection (ATR) mode, directly from the membrane surface. The spectra were recorded at a resolution of 4 cm^{-1} as an average of 16 scans. The membranes were washed in acetone to remove any contamination and dried before analysis.

2.3.3. Scanning electron microscopy/Energy-dispersive X-ray spectroscopy The surfaces and cross-sections of the membrane were characterized by scanning electron microscopy (SEM). The samples were coated with chromium under an argon atmosphere using an Emitech K575X peltier in order to make the samples conductive. The microscopic analyses were performed at 5 kV in a high resolution LEO1525 Karl Zeiss SEM. Energy-dispersive X-ray spectroscopy (EDX) was carried out using the same LEO1525 Karl Zeiss SEM at 20 kV. The EDX samples were also coated with chromium.

2.3.4. X-ray powder diffraction The X-ray powder diffraction patterns were acquired at room temperature on a PANalytical X'Pert Pro diffractometer using CuKα radiation (1.541 Å), with a Nickel filter, a fixed 10 mm mask, a 0.04 rad soller slit and divergence and antiscatter slits of 1/4° and 1/2° respectively. The data was collected between a 5 to 40° angular range in 2θ in continuous scan mode using a step size of 0.05° and a step time of 5 s.

2.3.5. Contact angle Contact angle measurements were performed with an Easy-Drop Instrument (manufactured by Kruess) at room temperature using the drop method, in which a drop of water was deposited on the surface of a membrane using a micropipette. The contact angle was measured automatically by a video camera using the drop shape analysis software. All membranes were washed with acetone to remove any contamination and were dried prior to measuring their contact angle. The removal of PEG conditioning agent was confirmed using ATR-FTIR.

2.3.6. BET surface area analysis PEG-400 conditioning agent was removed from the membranes using acetone. The removal of PEG conditioning agent was confirmed using ATR-FTIR. The membranes were dried at room temperature and then degassed overnight at 80 °C to further remove any traces of solvent from the membrane that may interfere with the adsorption of nitrogen onto the membrane surface. The BET surface areas of the membranes were then determined using a gas adsorption analyser (Tristar 3000, Micromeritics, Norcross, GA) which measured the membrane surface area based on nitrogen adsorption.

2.3.7. Atomic force microscopy The surface topographies of the membranes were characterized by tapping-mode atomic force microscopy (AFM) (Innova, Veeco, TESP-SS probes).

No alterations were made to the membranes before AFM was performed.

2.4. OSN experimental procedure

Each membrane (UF, MMM and ISG) was independently prepared two times and two membrane discs were tested from each membrane prepared. The reported results are the mean values of these measurements. All filtration experiments were carried out at 10 bar using a cross-flow filtration system. The effective area of each membrane was 14 cm^2, and at least 2 discs of each membrane were placed in an 8 cell cross-flow rig, which comprises 2 parallel sets of 4 membranes in series. The membranes were tested for 24 hours in order to ensure a steady permeance had been reached. The initial permeance and the final steady state membrane permeance were measured in order to calculate the membrane flux decline. The membrane permeance was calculated as given in **Equation 1**.

$$\boldsymbol{Permeance} = \frac{J}{\Delta P} = \frac{V}{\Delta P A t} = [\boldsymbol{L.m^{-2}.h^{-1}.bar^{-1}}] \qquad \textbf{(Eq. 1)}$$

The permeance of each membrane was obtained by measuring the solvent flux through the membrane (J) and dividing this by the applied pressure across the membrane (ΔP). The flux was calculated by measuring the volume of solution (V) that permeates through the membrane per unit area (A) per unit time (t). The model system for the solute rejection experiments comprised of a mixture of 1 $g.L^{-1}$ PS580 and PS1300 polystyrene markers as well as 0.1 $g.L^{-1}$ of methyl styrene dimer solution in acetone[37]. The rejection (R_j) of markers was found by measuring the concentration of each polystyrene oligomer in the permeate ($C_{p,i}$) and the feed ($C_{f,i}$), respectively and calculating the ratio of the molecules retained by the membrane. The equation to calculate membrane rejection can be found in **Equation 2**.

$$\boldsymbol{R_{j,i}} = \left(\mathbf{1} - \frac{C_{p,i}}{C_{f,i}}\right) \cdot \mathbf{100} = [\%] \qquad \textbf{(Eq. 2)}$$

Samples of polystyrene solution were taken from the feed and the permeate line of each of the tested membranes. Acetone was evaporated and the residue was re-dissolved in DMF. The HPLC analysis was based on the method previously reported by See-Toh et al[37]. Analysis of the polystyrene markers was undertaken using an Agilent HPLC system equipped with UV/Vis detector set at a wavelength of 264 nm and a Phenomenex C18 (300A, 250x4.6 mm) reverse phase column.

3. Results and discussion

3.1 Preparation of hybrid Polymer/MOF membranes

There is a visible colour difference between the ultrafiltration membrane (UF), the mixed matrix membrane (MMM) and the in-situ growth membrane (ISG), this can be seen in the images found in **Figure 3**. Unprocessed P84 powder is yellow, while HKUST-1 is blue. When HKUST-1 powder is added to the polymer dope solutions for MMM fabrication, the mix of blue and yellow from the HKUST-1 and the P84 respectively produce a green dope solution. The colour of the MMM remains green after the immersion precipitation process, indicating that the HKUST-1 particles remain lodged in the polymer matrix. The yellow P84 membrane turns blue when submerged in the blue HKUST-1 precursor solution during the formation of the ISG membrane. This change in colour is evidence that copper ions have been incorporated within the membrane matrix.

X-Ray Powder Diffraction (XRPD) was carried out on each membrane in order to prove that the colour change that occurs with the ISG membrane is due to the growth of HKUST-1. HKUST-1 is a crystalline material with a regular structure and a well-documented XRPD pattern[38, 39]. The XRPD pattern for pure HKUST-1 crystals are shown in **Figure 3**, the largest peaks are at 9.3°, 11.4° and 13.1°. The P84 UF membranes are semi-crystalline in structure. The polymer chains are randomly orientated throughout the membrane, and as such the XRPD pattern of the UF membrane is a smooth slope with no clear peaks. The XPRD patterns for both hybrid membranes, MMM and ISG, are a mixture of the features of P84 and the peaks of HKUST-1.

Table 1: Thickness, weight per square metre and density of membranes produced in this work.

	Thickness (µm)	Mass ($g.m^{-2}$)	Density ($g.cm^{-3}$)
UF	102 ± 2	54 ± 2	0.53 ± 0.02
MMM	99 ± 2	60 ± 3	0.61 ± 0.02
ISG	107 ± 3	82 ± 2	0.76 ± 0.01

XRPD proved the presence of the HKUST-1 in the membranes but as an analytical method it is only qualitative. In order to obtain quantifiable data about the amount of HKUST-1 in the membranes, the thickness, mass and density of the hybrid membranes were measured and compared with the polymer UF membrane. The masses reported in **table 1** represent the mass of the membrane, minus the weight of the polypropylene backing. Polypropylene was independently submerged in HKUST-1 precursor solution and no significant change in mass was measured.

The difference in thickness between the membranes is negligible. The largest changes can be seen in the weight and the density of the membranes. There is a large increase in weight once HKUST-1 is grown in the ISG membrane, and also a corresponding increase in the density of the membrane. The mass percentage of HKUST-1 in the ISG membrane was estimated based on the increased weight of the membrane using **Equation 3**.

$$\boldsymbol{MOF}(\%)_{\boldsymbol{ISG}} = \frac{M_{(ISG)} - M_{(UF)}}{M_{(ISG)}} \times \mathbf{100} \qquad \textbf{(Eq. 3)}$$

Where the $MOF(\%)_{ISG}$ is the percentage by mass of HKUST-1 in the ISG membrane and $M_{(ISG)}$ and $M_{(UF)}$ the mass of the ISG and the UF membrane respectively. Using **Equation**

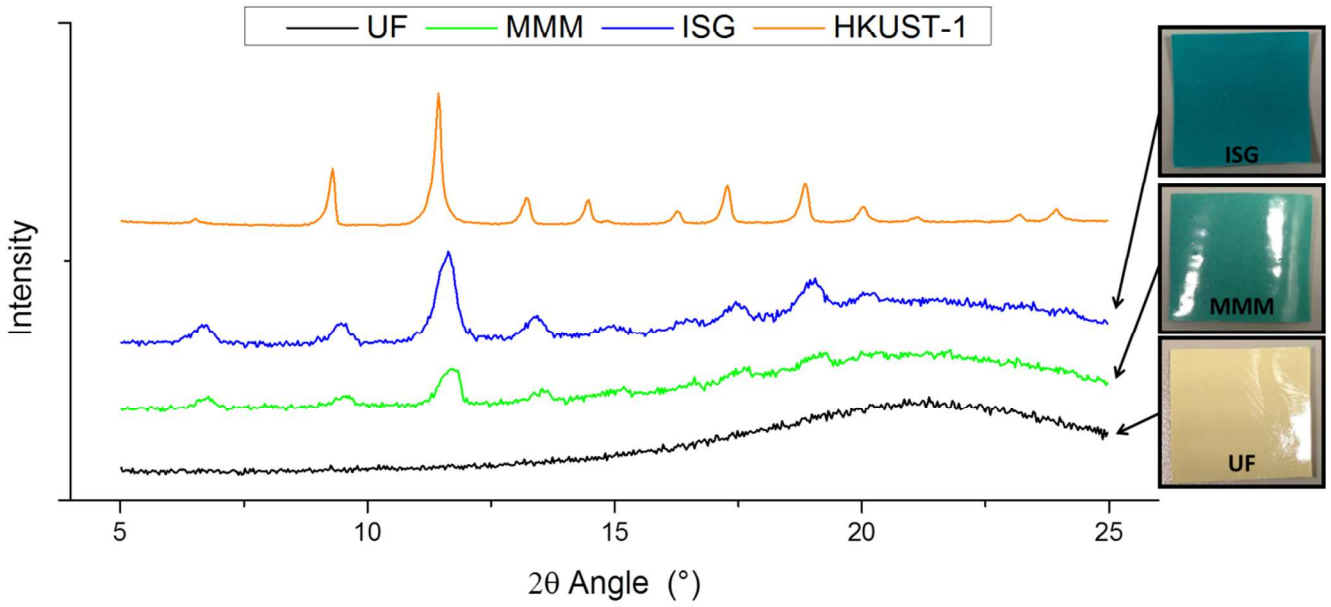

Figure 3: X-Ray Powder Diffraction (XRPD) data for membranes showing characteristic HKUST-1 peaks blended with the profiles of the P84 UF polymer membrane

3 the MOF(%) in the ISG membrane is calculated to be 33%. The increase in weight and density of the ISG membrane, along with the negligible change in thickness, indicate that HKUST-1 mostly grows within the pre-existing pores in the UF membrane. The overall porosity of the original UF can be calculated using **Equation 4**.

$$\varphi = 1 - \frac{\rho_{(UF)}}{\rho_{(P84)}} \qquad \textbf{(Eq. 4)}$$

Where φ is the porosity and $\rho_{(UF)}$ and $\rho_{(P84)}$ are the density of the UF membrane and the P84 polymer respectively. The density of P84 is 1.34 g cm^{-3}[40], thus the calculated porosity of the UF membrane is 0.6. Using the change in membrane density between the UF and the ISG membrane the extent of pore filling by MOF in the ISG membrane can be calculated using **Equation 5**.

$$\textit{Pore filling by HKUST}\ (\%) = \frac{\left(\frac{\rho_{(ISG)} - \rho_{(UF)}}{\rho_{(HKUST-1)}}\right)}{\varphi} \qquad \textbf{(Eq. 5)}$$

Where $\rho_{(ISG)}$ and $\rho_{(HKUST-1)}$ are the densities of the ISG membrane and HKUST-1 respectively, and φ is the porosity of the UF membrane. Using a density of 1.22 g cm^{-3} for HKUST-1 [41], the pore filling by HKUST-1 is 31% based on the additional assumption that no MOF grows outside of the porous structure of the polymer membrane.

The mass of HKUST-1 added to the dope solution for the MMM was at a ratio of 1:5 MOF to polymer, this equates to 17% MOF by weight. The HKUST-1 particles are denser than the surrounding polymer membrane; therefore the percentage of HKUST-1 retained by the membrane can be calculated using the observed increase in density. The percentage mass of HKUST-1 retained by the MMM during the casting process can be calculated using **Equation 6**.

$$\textit{MOF}(\%)_{MMM} = \frac{\rho_{(MMM)} - \rho_{(UF)}}{\rho_{(HKUST-1)} - \rho_{(UF)}} \qquad \textbf{(Eq. 6)}$$

Where MOF(%)$_{MMM}$ is the percentage by mass of HKUST-1 in the MMM and $\rho_{(MMM)}$ is the density of the MMM. Using this calculation the mass of HKUST-1 in the MMM amounts to 12%. The observed reduction in MOF(%) can be attributed to large HKUST-1 particles settling towards the bottom of the dope solution, and therefore not being incorporated into the membrane efficiently.

As a result of its microporous structure, HKUST-1 has a large internal surface area. The BET surface area of HKUST-1 was measured as 1176 m^2.g^{-1}, which is in accordance with values found in literature[42, 43]. The BET surface area of the UF membrane is 10.85 ± 0.02 m^2.g^{-1}. The BET surface area of the MMM is 10.17 ± 0.02 m^2.g^{-1}. The ISG membrane has the highest BET surface area, 26.1 ± 0.2 m^2.g^{-1}. The low BET surface areas observed for the hybrid membranes are probably due to the heating and drying of the membranes required for the BET analysis. This would cause the collapse of the polymer matrix, sealing the HKUST-1 within the membrane. The BET surface area for the ISG membrane is higher than for the MMM, indicating that the accessibility of the HKUST-1 micropores is higher in ISG membranes than MMM.

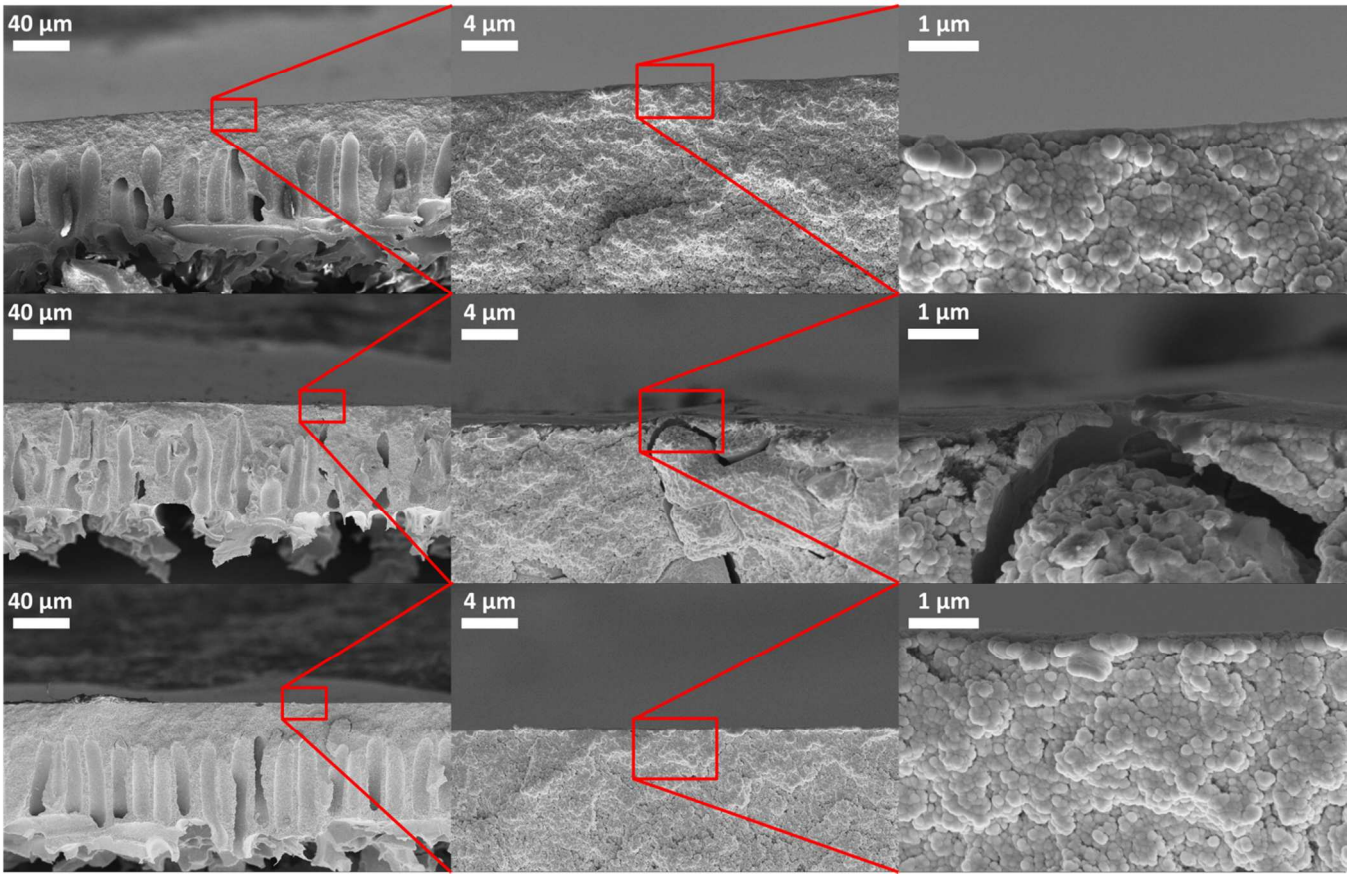

Figure 4: SEM images of the cross-section of membranes (top) UF, (middle) MMM and (bottom) ISG

3.2 HKUST-1 Distribution in Hybrid Membranes

The membranes each have the typical structure of integrally skinned asymmetric polymer membranes formed via phase inversion, with dense top layers, spongy support structures in the middle of the membrane and macrovoids at the bottom of the membranes. **Figure 4** shows SEM images from each of the membranes types. Visually there is very little difference between the UF and ISG membranes, the individual HKUST-1 crystals in the ISG membrane cannot be seen, suggesting that the crystal sizes must be on the nanometre scale. In the MMM the HKUST-1 crystals can be clearly seen, as they are on the micron scale. The presence of the HKUST-1 crystals in the MMM has caused distortion of the macrovoids in the membrane.

The presence of copper in the membranes was measured using EDX analysis. As HKUST-1 contains 31.5% copper by weight and copper is not found in P84, the copper signal is used to show the distribution of HKUST-1 in the hybrid membranes. The distribution of copper throughout the cross-section the hybrid membranes can be found in **Figure 5.** The height of the red lines in Figure 5 reflect the relative 'counts' of copper throughout the cross-section of the membrane. The presence of copper can be found throughout the cross-section of the ISG membrane at roughly similar values. For the MMM however the copper signal can only be found where the HKUST-1 crystals can be seen. **Figure 5** shows that the distribution of HKUST-1 throughout ISG membranes is even and continuous while the distribution of MOF in MMMs is discrete.

3.3 The surface properties of hybrid polymer/MOF membranes

Attenuated total reflection Fourier Transform-Infrared (ATR-FTIR) was used to analyse the chemical structure of the surface of the membranes. **Figure 6** shows that the ISG membrane IR signal follows the same characteristic peaks as the HKUST-1 powder. The characteristic absorbance at 740, 1380 and 1450 cm^{-1} are in accordance with those found in literature[44]. The MMM shows no IR evidence of HKUST-1 at the membrane surface, and closely follows the IR signal of the UF membrane. ATR-FTIR can penetrate materials up to 5 microns in depth, so though the HKUST-1 material is located in the MMM, the MOF crystals are not often found at the membrane surface. The lack of HKUST-1 at the membrane surface can be

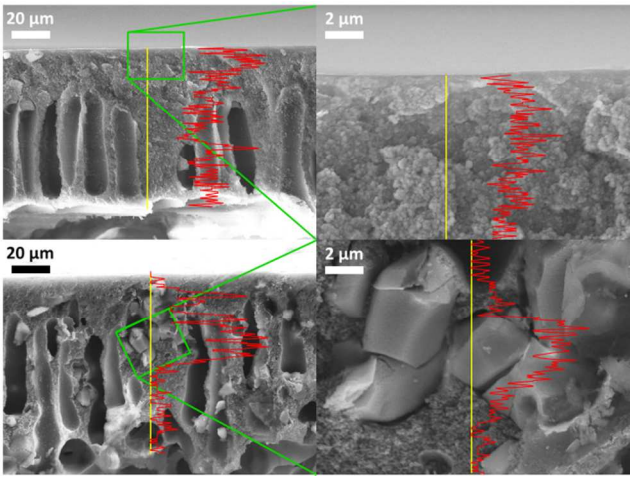

Figure 5: SEM/EDX images of the cross-section of membranes (top) ISG and (bottom) MMM

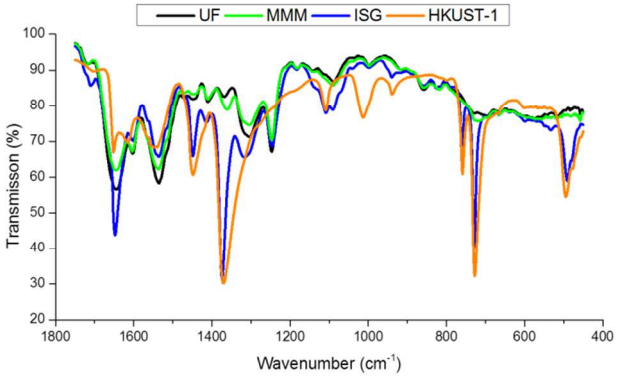

Figure 6: ATR-FTIR data from the membrane surface showing large peaks associated with the HKUST-1 structure shown for the ISG sample only

explained by the tendency of the HKUST-1 particles to sink during the membrane casting process. The MOF particles are covered by the polymer dope solution before phase inversion, disfavouring siting of HKUST-1 at the membrane surface.

Copper signals from the surfaces of the hybrid membranes, ISG and MMM, were obtained using SEM/EDX, the presence of copper was used as evidence of the presence of HKUST-1. As in Figure 5, the height of the red lines in **Figure 7** reflect the relative 'counts' of copper across the surface of the membranes. **Figure 7** shows that the surface of the ISG membrane is evenly covered in HKUST-1 crystals, whereas for the MMM there is only a single a peak where a single crystal of HKUST-1 is protruding from the membrane surface. Confirming the data shown in Figure 6 indicating that the surface of the ISG membrane is covered in HKUST-1, whereas

AFM was used to measure changes in the membrane topology caused by the addition of HKUST-1 to polymer membranes. It can be seen in **figure 8** that the surface of the UF membrane is mostly flat and featureless. The surface of the MMM is also mostly flat, though has large defects in the

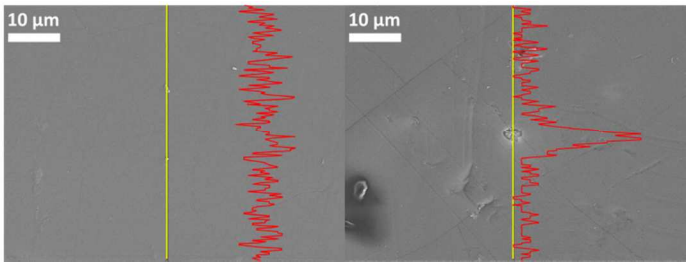

Figure 7: SEM/EDX of (left) ISG membrane surface and (right) MMM membrane surface

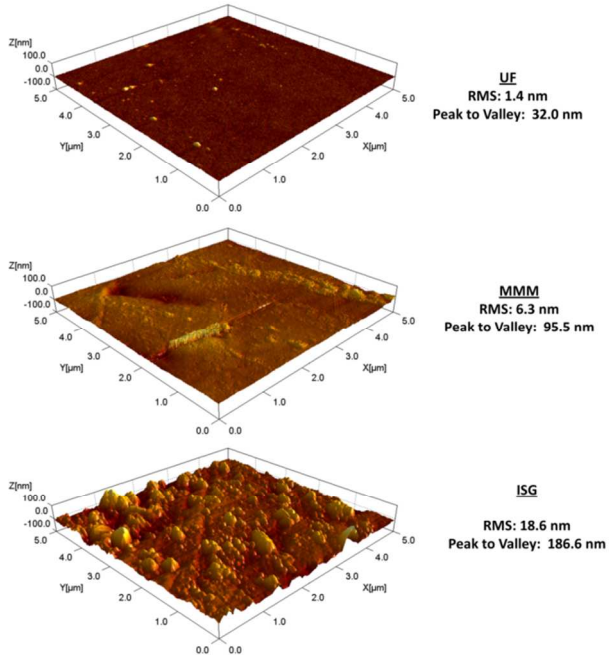

Figure 8: AFM images of the surface of membranes (top) UF (middle) MMM and (bottom) ISG, the aspect ratio of the AFM images is 1:1:3 for the X:Y:Z coordinates.

surface, caused by the disruption of the membrane by HKUST-1 particles in the membrane formation process. This confirms the ATR-FTIR and EDX data for the MMM. The surface of the MMM remains mostly P84, but the topology has been changed due to the presence of MOF particles below the membrane surface. The most comprehensive change to the membrane surface is observed in the ISG membrane. The flat surface of the UF membrane has completely changed in topology. The HKUST-1 has grown across the surface of the membrane, introducing large features, up to in 100 nm in height, across the membrane surface. HKUST-1 covers the top layer of the ISG membrane, which indicates that the MOF should have a larger influence on the selective properties of the ISG membrane than the MMM, whose surface remains largely polymer.

The water contact angle of the UF membrane was measured as 62±1°, proving that the membrane is fairly hydrophilic in nature. The contact angles for both the hybrid HKUST-1 membranes, MMM and ISG, were 58±4° and 65±2°

respectively. The addition HKUST-1 appears to have little influence on the hydrophillicity of P84 UF membranes.

3.4. Membrane performance

3.4.1 Performances of hybrid polymer/MOF membranes (ultrafiltration supports) The permeance data from the two hybrid membranes (MMM and ISG) and the polymer support membrane (UF) are reported in **Table 2**. The UF membrane has the highest flux (177 L m^{-2} h^{-1} bar^{-1}) and the highest flux decline (18%). Polymer nanofiltration membranes (Molecular weight cut-off (MWCO) ≈ 1700 g mol-1) in the same experimental set-up had an initial permeance of 5.6 L m^{-2} h^{-1} bar^{-1} and a flux decline of 31%, showing, that even with a low initial permeance, flux decline is
still an issue for integrally skinned asymmetric polymer membranes. The MMM had the second highest permeance, and a lower flux decline than the polymeric membranes. The ISG membranes had the lowest flux decline of all the membranes tested with a value of 2%. The 9 times reduction in flux decline observed in ISG membrane compared to the UF membrane is probably due to the additional rigidity of the HKUST-1 resisting the effects of compaction. In the case of the ISG membrane the HKUST-1 fills the pores in the polymer matrix; this impedes the rearrangement of the polymer chains on a microscopic scale, leading to negligible flux decline. The flux decline of the MMM is slightly larger than that of the ISG membrane. Here any reduction in flux decline is probably due to the macroscopic mechanic properties of the membrane. The large HKUST-1 crystals in the MMM act as a rigid support to the whole membrane structure, reducing the compression of the membrane by the applied pressure, though polymer chains can still rearrange on a microscopic scale.

Table 2: Pure solvent flux of membranes with calculated flux decline in acetone

	Initial Acetone Permeance (L m^{-2} h^{-1} bar^{-1})	Final Acetone Permeance (L m^{-2} h^{-1} bar^{-1})	Flux Decline
UF	217 ± 1.8	177 ± 14	18%
MMM	99.0 ± 30	93.2 ± 32	6%
ISG	18.4 ± 4.2	18.0 ±3.6	2%

The rejection performances of the membranes can be found in **Figure 9**. The UF membrane has a very flat profile with the lowest rejections. Both the ISG and MMM have higher rejections than the UF membrane, with the highest rejections achieved by the ISG membrane.

It can be seen in **Figure 9** that the error bars on the rejection curves of MMM are significantly larger than the error bars of the UF and ISG membranes. This can be attributed to the structural nature of the MMMs. The structure of the MMMs is naturally less homogenous than the polymer membranes and the ISG membranes due to their fabrication methodology. The random dispersion of discrete HKUST-1 particles in the membranes causes some areas of the membrane sheet to be richer in MOF than others. This leads to membranes coupons having differing membrane performances.

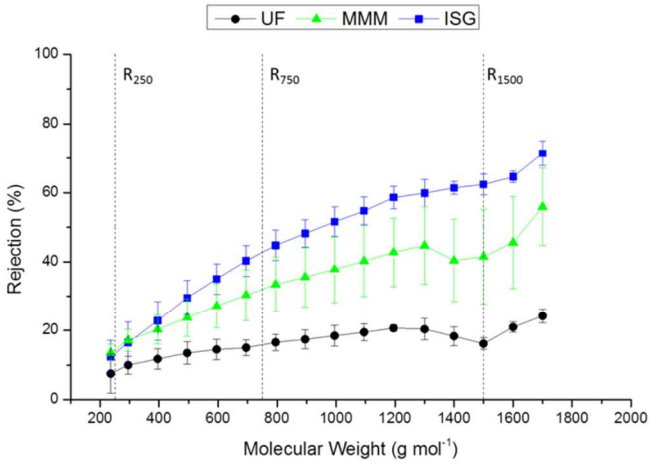

Figure 9: MWCO curves for P84 membranes (UF), mixed matrix membranes (MMM) and *in-situ* growth MOF membranes (ISG) tested at 10 bar with polystyrene in acetone solvent. Mean data for each membrane plotted, error bars show one standard deviation

Further analysis of the polystyrene rejection curves can be found in **Table 3**. Rejections of the polystyrene markers were calculated for low range molecular weight (MW) solutes, 250 g mol^{-1}, mid-range MW solutes, 750 g mol^{-1}, and high MW solutes, 1500 g mol^{-1}.

The rejection and permeance data suggests that the addition of HKUST-1 to polymer membranes both via *in-situ* growth and dispersion of *ex-situ* grown crystals in the polymer dope changes the transport properties of the membranes.

Table 3: Calculated rejections for the membranes in the nanofiltration range at low MW (R_{250}), mid-range MW (R_{750}) and high MW (R_{1500})

	UF (%)	MMM (%)	ISG (%)
R_{250}	8.1	14.4	13.4
R_{750}	15.9	32.0	42.7
R_{1500}	16.2	41.5	62.4

The rejection and permeance performance of the ISG membrane would appear to confirm that HKUST-1 growth occurs within the pre-formed porous structure of the UF membrane. HKUST-1 has a pore-filling effect on ISG membranes, slowing solvent transport, and reducing the average pore size of the selective layer of the membranes. However it can be surmised that perfect MOF coverage throughout the membrane is not yet achievable as the small pore size of the HKUST-1 should retain all but the smallest polystyrene oligomers. The growth of HKUST-1 in the ISG membrane alters the existing pores of the polymer membrane,

and the MOF phase has been shown to be more continuous than the MMM.

3.4.2 Performances of hybrid polymer/MOF membranes (dense polymer supports) In order to improve the performance of the hybrid polymer/MOF membranes, the two fabrication methodologies were tested with denser membranes. Denser membranes have slightly less porous structures leading to higher solute retentions. By improving the performance of the base UF membrane to that of a dense support membrane, UF(D), the overall performance of the hybrid membranes could also be improved.

Table 4: Thickness, mass per square metre, density and surface area of the denser membranes used in this study

	Thickness (µm)	Mass ($g.m^{-2}$)	Density ($g.cm^{-3}$)
UF(D)	67 ± 1	43 ± 3	0.64 ± 0.05
MMM(D)	70 ± 5	47 ± 6	0.67 ± 0.09
ISG(D)	65 ± 3	63 ± 2	0.97 ± 0.06

The thickness, mass and density of the dense polymer support membrane, UF(D) and the subsequent hybrid membranes, MMM(D) and ISG(D) are reported in **Table 4**. The dense membranes are 30 to 40 µm thinner than the original membranes. The ISG(D) membrane has a calculated HKUST-1 weight percentage of 32%, which is similar to that observed in the original ISG membrane. The UF(D) has a calculated porosity of 0.52, making it less porous than the original UF membrane. The calculated pore filling of the ISG(D) membrane is 52%, compared to 31% with the original ISG membrane.

Table 5: Pure solvent flux of membranes with calculated flux decline in acetone

	Initial Acetone Permeance ($L\ m^{-2}\ h^{-1}\ bar^{-1}$)	Final Acetone Permeance ($L\ m^{-2}\ h^{-1}\ bar^{-1}$)	Flux Decline
UF(D)	215 ± 49	120 ± 40	44%
MMM(D)	70.7 ± 4.5	61.7 ± 2.1	13%
ISG(D)	15.4 ± 2.1	15.1 ± 2.7	2%

The rejection and permeance data for the dense membranes follows the same trends as original UF, MMM and ISG membranes. The permeance data for the dense membranes can be found in **Table 5**, and the rejection data can be found in **Figure 10**. The increased density of the UF(D) membrane leads to higher rejections of the polystyrene oligomers and a decrease in the final acetone permeance. Flux decline remains an issue with the UF(D), indicating that even dense polymer supports suffer compaction and flux decline. In fact the dense membrane suffers from even higher flux decline than the original UF membrane. The permeance of the MMM(D) is, 61.7 L m^{-2} h^{-1} bar^{-1}, which is lower than the original MMM.. The MMM(D) has a flux decline of 13%, twice as large as the original MMM, though the flux decline is still less than both the UF and the UF(D). The ISG(D) has the highest rejection of all the membranes, and permeance and flux decline values of 15.1 L m^{-2} h^{-1} bar^{-1} and 2% respectively.

It can be seen in **Figure 10** that, as with the original MMM, the MMM(D) rejection curve also exhibits larger error bars than the UF(D) and ISG (D) membranes. This increase in error is once again attributed to the lower homogeneity of the MMM(D) structure compared to the UF(D) and the ISG(D) membranes.

The decreases in permeance for the dense membranes compared to the original membranes are 32% for the UF membranes, 33% for the MMMs and 16% for the ISG membranes. The decrease in permeance can be explained by the reduced porosity of the polymer membranes.

Increasing the density improves the rejection performance of polymer membranes. The hybrid polymer/MOF membranes produced with dense membranes also have improved rejections. While the changes in rejection and permeance for the MMMs are similar to the changes observed for the UF membranes, the changes for the ISG membranes are more favourable. The reduction in permeance of the ISG(D) is less than the other membranes while increase in rejection is greater.

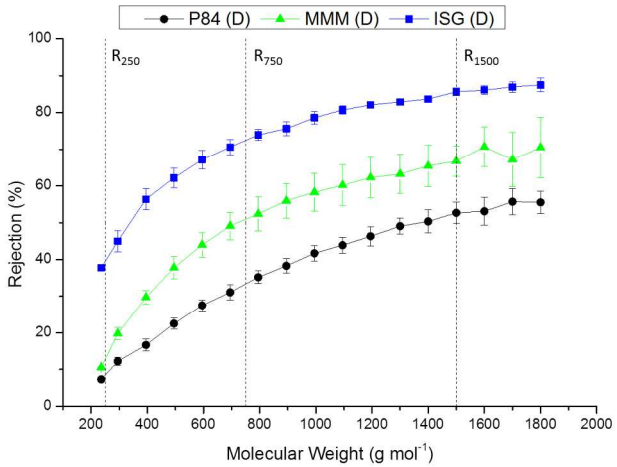

Figure 10: MWCO curves for P84 membranes (UF), mixed matrix membranes (MMM) and *in-situ* growth MOF membranes (ISG) tested at 10 bar with polystyrene in acetone solvent. Mean data for each membrane plotted, error bars show one standard deviation.

Table 3: Calculated rejections for the membranes in the nanofiltration range at low MW (R_{250}), mid-range MW (R_{750}) and high MW (R_{1500})

	UF (D)	MMM (D)	ISG (D)
R_{250}	8.4	12.7	39.5
R_{750}	33.3	50.9	72.4
R_{1500}	52.6	66.7	85.6

4. Conclusions

This work compared and contrasted two hybrid polymer/MOF membrane fabrication methodologies, the mixed matrix membrane (MMM) approach and in-situ growth (ISG) of MOFs in pre-existing polymer membrane pores. The hybrid membranes were characterized by SEM, EDX, FTIR, XRPD, AFM and BET and the differences in structure of the membranes were explored. It was shown that the ISG methodology produces membranes with an even MOF distribution throughout the membrane and across the membrane surface. This differs significantly from the structure of the MMM, which contained discrete particles of HKUST-1 in a continuous polymer phase. The OSN performances of the ISG and MMM membranes were tested and compared to the control polymer UF membrane. Comparison of the solute rejection curves clearly indicated the performance enhancing effect of the presence of HKUST-1. MMMs were shown to have improved solute rejections above plain polymeric membranes, while the ISG approach improved the polystyrene oligomer rejections even further. MOF addition was also found to have a positive influence on flux decline, with the ISG membranes having the lowest fall in permeance over time. It was also shown that the performance of hybrid polymer/MOF membranes can be further improved by incorporating HKUST-1 into dense polymer support membranes.

The analytical methods used character the structure of the hybrid membranes, along with the OSN performance data, indicate that ISG membranes have several advantages over MMMs. These advantages include, an even spread of HKUST-1 throughout the cross-section and across the surface of the ISG membranes, proved by EDX and AFM, higher accessibility to the HKUST-1 pores, proved by BET analysis and reduced flux decline. The ISG hybrid membrane fabrication approach could be used in the future to produce gas separation membranes and membranes used for combined catalysis and separation processes.

Future work in the area of ISG membranes should focus on improving the rejection and permeance performances of the membranes. Incorporation of chemical modification agents to improve the adhesion between the polymer and the MOF phases is one method that could lead to improved membrane rejections. Once defect free ISG membranes can be fabricated, development of ISG membranes containing MOFs other than HKUST-1 could be used to exert more control on the membrane rejections. Use of MOFs with different pore sizes would allow for control of the molecular weight cut-offs of ISG membranes based purely on the pore size of the chosen MOF.

Acknowledgements

The authors would like to acknowledge financial support from the EPSRC and the Pharmacat consortium.

Notes and references

[a] Department of Chemical Engineering, Imperial College, London SW7 2AZ, UK.

[b] Department of Chemistry, Imperial College, London SW7 2AZ, UK

∗ Corresponding author: Tel.: +44-20-7594-5582. *E-mail address:* a.livingston@imperial.ac.uk

1. Vandezande, P., L.E.M. Gevers, and I.F.J. Vankelecom, *Solvent resistant nanofiltration: separating on a molecular level.* Chemical Society Reviews, 2008. **37**(2): p. 365–405. (DOI: 10.1039/B610848M)
2. See-Toh, Y.H., F.W. Limb, and A.G. Livingston, *Polymeric membranes for nanofiltration in polar aprotic solvents.* Journal of Membrane Science, 2007(301): p. 3–10.
3. Vanherck, K., et al., *Cross-linked polyimide membranes for solvent resistant nanofiltration in aprotic solvents.* Journal of Membrane Science, 2008. **320**: p. 468–476.
4. See-Toh, Y.H., F.C. Ferreira, and A.G. Livingston, *The influence of membrane formation parameters on the functional performance of organic solvent nanofiltration membranes.* Journal of Membrane Science, 2007. **299**: p. 236–250.
5. See-Toh, Y.H., M. Silva, and A. Livingston, *Controlling molecular weight cut-off curves for highly solvent stable organic solvent nanofiltration (OSN) membranes.* Journal of Membrane Science, 2008. **324**: p. 220–232.
6. Gibbins, E., et al., *Observations on solvent flux and solute rejection across solvent resistant nanofiltration membranes.* Desalination, 2002. **147**(1-3): p. 307–313.
7. Siddique, H., et al., *Mixed matrix membranes fo rorganic solvent nanofiltration.* Journal of Membrane Science, 2014. **452**: p. 354–366. (DOI: 10.1016/j.memsci.2013.10.012)
8. Soroko, I. and A. Livingston, *Impact of TiO2 nanoparticles on morphology and performance of crosslinked polyimide organic solvent nanofiltration (OSN) membranes.* Journal of Membrane Science, 2009. **343**(1-2): p. 189–198. (DOI: 10.1016/j.memsci.2009.07.026)
9. Basu, S., A. Cano-Odena, and I.F.J. Vankelecom, *Asymmetric Matrimid®/[Cu3(BTC)2] mixed-matrix membranes for gas separations.* Journal of Membrane Science, 2010. **362**: p. 478-487.
10. Hu, J., et al., *Mixed-Matrix Membrane Hollow Fibers of Cu3(BTC)2 MOF and Polyimide for Gas Separation and Adsorption.* Industrial Chemical Engineering Research, 2010(49): p. 12605–12612.
11. Car, A., C. Stropnik, and K.-V. Peinemann, *Hybrid membrane materials with different metal–organicframeworks (MOFs) for gas separation.* Desalination, 2006. **200**: p. 424-426.
12. Basu, S., A. Cano-Odena, and I.F.J. Vankelecom, *MOF-containing mixed-matrix membranes for CO2/CH4 and CO2/N2 binary gas mixture separations.* Separation and Purification Technology, 2011. **81**: p. 31-40.
13. Aroon, M.A., et al., *Performance studies of mixed matrix membranes for gas separation: A review.* Separation and Purification Technology, 2010. **75**: p. 229-242.
14. Perez, E.V., et al., *Mixed-matrix membranes containing MOF-5 for gas separations.* Journal of Membrane Science, 2009. **328**: p. 165–173.
15. Zhang, Y., et al., *Gas permeability properties of Matrimid® membranes containing the metal-organic framework Cu–BPY–HFS.* Journal of Membrane Science, 2008. **313**: p. 170–181.

16. Adams, R., et al., *Metal organic framework mixed matrix membranes for gas separations.* Microporous and Mesoporous Materials, 2010. **131**: p. 13-20.
17. Dong, G., H. Lia, and V. Chen, *Challenges and opportunities for mixed-matrix membranes for gas separation.* Journal of material Chemistry A, 2013. **1**: p. 4610–4630.
18. Fang, Q., et al., *Porous Metal-Organic Frameworks*, in *Comprehensive Nanoscience and Technology*. 2010, Elsevier B.V.
19. Rowsell, J.L.C. and O.M. Yaghi, *Metal–organic frameworks: a new class of porous materials.* Microporous and Mesoporous Materials, 2004. **73**: p. 3–14.
20. Chae, H.K., et al., *A route to high surface area, porosity and inclusion of large molecules in crystals.* Nature, 2003. **427**: p. 523-527. (DOI: 10.1038/nature02311)
21. Farha, O.K., et al., *Designing Higher Surface Area Metal–Organic Frameworks: Are Triple Bonds Better Than Phenyls?* Journal of the American Chemical Society, 2012. **134**(24): p. 9860–9863. (DOI: 10.1021/ja302623w)
22. Martin, R.L. and M. Haranczyk, *Exploring frontiers of high surface area metal–organic frameworks.* Chemical Science, 2013(4): p. 1781-1785. (DOI: 10.1039/C3SC00033H)
23. Basu, S., et al., *Solvent resistant nanofiltration (SRNF) membranes based on metal-organic frameworks.* Journal of Membrane Science, 2009. **344**: p. 190–198.
24. Sorribas, S., et al., *High Flux Thin Film Nanocomposite Membranes Based on Metal−Organic Frameworks for Organic Solvent Nanofiltration.* Journal of the American Chemical Society, 2013. **135**(40): p. 15201–15208. (DOI: 10.1021/ja407665w)
25. Powell, C.E. and G.G. Qiao, *Polymeric CO2/N2 gas separation membranes for the capture of carbon dioxide from power plant flue gases.* Journal of Membrane Science, 2006. **279**(1-2): p. 1-49.
26. Chung, T.-S., L.Y. Jiang, and S.K. Yi Lia, *Mixed matrix membranes (MMMs) comprising organic polymers with dispersed inorganic fillers for gas separation.* Progess in Polymer Science, 2007. **32**: p. 483–507.
27. Bouma, R.H.B., et al., *Permeation through aheterogeneous membrane: the effect of the dispersed phase.* Journal of Membrane Science, 1997. **128**: p. 141-149.
28. Moore, T.T., et al., *Hybrid Membrane Materials Comprising Organic Polymers with Rigid Dispersed Phases.* AIChE Journal, 2004. **50**(2): p. 311-321.
29. Vu, D.Q., W.J. Koros, and S.J. Miller, *Mixed matrix membranes using carbon molecular sieves II. Modeling permeation behavior.* Journal of Membrane Science, 2003. **211**: p. 335-348.
30. Hashemifard, S.A., A.F. Ismail, and Matsuura, *Prediction of gas permeability in mixed matrix membranes using theoretical models.* Journal of Membrane Science, 2010. **347**: p. 53-61.
31. Cao, L., et al., *A highly permeable mixed matrix membrane containing CAU-1-NH2 for H2 and CO2 separation.* Chemical Communication, 2013(49): p. 8513-8515. (DOI: 10.1039/c3cc44530e)
32. Ge, L., et al., *Mixed matrix membranes incorporated with size-reduced Cu-BTC for improved gas separation.* Journal of MAterials Chemistry A, 2013. **1**(21): p. 6350–6358. (DOI: 10.1039/C3TA11131H)
33. Gascon, J., S. Aguado, and F. Kapteijn, *Manufacture of dense coatings of Cu3(BTC)2 (HKUST-1) on a-alumina.* Microporous and Mesoporous Materials, 2008. **113**: p. 132–138.
34. Majano, G. and J. Perez-Ramrez, *Room Temperature Synthesis and Size Control of HKUST-1.* Helvetica Chimica Acta, 2012. **95**(11): p. 2278–2286.
35. Li, Y.-S., et al., *Molecular Sieve Membrane: Supported Metal–Organic Framework with High Hydrogen Selectivity.* Angewandte Cemie International Edition, 2010. **49**(548 –551).
36. Li, Z.-Q., et al., *Ultrasonic synthesis of the microporous metal–organic framework Cu3(BTC)2 at ambient temperature and pressure: An efficient and environmentally friendly method.* Material Letters, 2009. **63**(1): p. 78-80.
37. See-Toh, Y.H., et al., *In search of a standard method for the characterisation of organic solvent nanofiltration membranes.* Journal of Membrane Science, 2007(291): p. 120–125.
38. Khan, N.A. and S.H. Jhung, *Facile Syntheses of Metal-organic Framework Cu3(BTC)2(H2O)3 under Ultrasound.* Bulletin of the Korean Chemical Society, 2009. **30**(12): p. 2921-2926.
39. Schlichte, K., T. Kratzke, and S. Kaskel, *Improved synthesis, thermal stability and catalytic properties of the metal-organic framework compound Cu3(BTC)2.* Microporous and Mesoporous Materials, 2004. **73**: p. 81–88.
40. GmbH, H.P.P., *P84 Polyimide Datasheet*, H.P.P. Inc, Editor. 1997.
41. Chui, S.S.-Y., et al., *A Chemically Functionalizable Nanoporous Material [Cu3(TMA)2(H2O)3]n.* Science, 1999. **283**(5405): p. 1148-1150 (DOI: 10.1126/science.283.5405.1148)
42. Li, Y. and R.T. Yang, *Hydrogen Storage in Metal-Organic and Covalent-Organic Frameworks by Spillover.* AIChE Journal, 2008. **54**(1): p. 269-279. (DOI: 10.1002/aic.11362)
43. Chen, H., et al., *Investigation on Hydrogenation of Metal−Organic Frameworks HKUST-1, MIL-53, and ZIF-8 by Hydrogen Spillover.* Journal of Physical Chemistry, 2013. **117**(15): p. 7565–7576. (DOI: 10.1021/jp401367k)
44. Janssens, N., et al., *Recovery and reuse of heteropolyacid catalyst in liquid reaction medium through reversible encapsulation in Cu3(BTC)2 metal–organic framework.* Chemical Science, 2012. **3**(6): p. 1847-1850.

